THE JOURNAL OF PHYSICAL CHEMISTRY B

Article

pubs.acs.org/JPCB

Multilayer Formation of the Fluoroalkanol–ω-Hydrogenated Fluorocarbon Mixture at the Hexane/Water Interface Studied by Interfacial Tensiometry and X-ray Reflection

Takanori Takiue,*[,†] Takuya Tottori,[†] Kazuo Tatsuta,[†] Hiroki Matsubara,[†] Hajime Tanida,[‡] Kiyofumi Nitta,[‡] Tomoya Uruga,[‡] and Makoto Aratono[†]

[†]Department of Chemistry, Faculty of Sciences, Kyushu University, Fukuoka 812-8581, Japan

[‡]Japan Synchrotron Radiation Research Institute, Hyogo 679-5198, Japan

ABSTRACT: Novel multilayer formation of fluorocarbon compounds at the hexane/water interface was investigated from the viewpoint of intermolecular interaction and miscibility of molecules in the adsorbed film. The two kinds of mixed systems were employed: 1*H*,1*H*,2*H*,2*H*-perfluorododecanol (FC12OH)−1*H*-perfluorodecane (HFC10) (System A) and 1-icosanol (C20OH)−HFC10 (System B). The interfacial tension γ between the hexane solution and water was measured as a function of total concentration m and the composition of HFC10 in the mixture X_2 at 298.15 K under atmospheric pressure. X-ray reflectivity (XR) measurement was performed at BL37XU in SPring-8 as a function of scattering vector $\mathbf{Q}_z$. In both systems, the γ vs m curves except for the pure HFC10 system have a break at low concentrations, which corresponds to the gaseous−condensed monolayer transition for System A and the expanded−condensed monolayer for System B. The remarkable difference between the two systems was that the curves in a limited bulk composition range ($0.45 \leq X_2 \leq 0.9$) of System A show another break at high concentrations close to the solubility limit. The total interfacial density above this break point was around 7−11 μmol m^{-2}, suggesting the spontaneous molecular piling to form a multilayer. The phase diagrams of adsorption in the condensed monolayer indicated that the film composition of HFC10 is negative in System B but definitely positive above $X_2 \geq 0.45$ in System A. This clearly shows that HFC10 molecules are miscible with FC12OH but immiscible with C20OH in the condensed monolayer. Thus, it is likely that the mixing of HFC10 with FC12OH in the condensed monolayer induces multilayer formation. The X-ray reflectivity normalized by Fresnel reflectivity R/R_F vs $\mathbf{Q}_z$ plot in the condensed monolayer of System A was fitted by a one-slab model with uniform electron density and thickness. The electron density profile was almost the same as that of the pure FC12OH system. The plot in the multilayer, on the other hand, was fitted well by the two-slab model with different electron densities and thicknesses. The electron density profile showed that the multilayer consists of two layers, one of which has slightly higher electron density than the bulk hexane phase and piles on the lower layer with almost the same electron density as the condensed FC12OH monolayer.

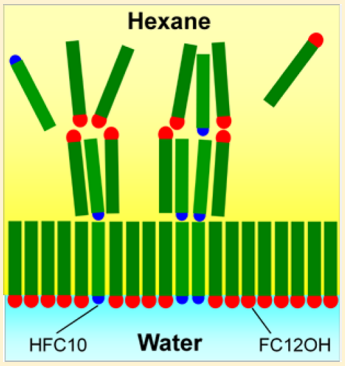

INTRODUCTION

Many studies have paid attention to the adsorption behavior of various surface-active substances at soft interfaces such as gas/liquid and liquid/liquid interfaces from the viewpoints of basic sciences as well as practical applications. Among others, fluorocarbon (FC) compounds show characteristic behaviors at the hydrocarbon (HC)/water interface due to the specific properties of the FC chain such as (i) a large polarization effect induced by a strong electronegative nature of the fluorine atom, (ii) the weak mutual interaction with the HC chain, and (iii) the rigidity of the hydrophobic chain and so on.[1−3] We have also explored the adsorption behavior of FC compounds at the hexane/water and air/water interfaces mainly by interfacial tensiometry and synchrotron X-ray reflection (XR).

The substitution of a fluorine atom of the terminal position of the FC chain into a hydrogen atom produces a terminal dipole (ω-dipole) and therefore is expected to affect appreciably the adsorption at the interface as well as the aggregation behavior in the bulk solution.[4−7] In the study of the surface adsorption and micelle formation in the aqueous solution of FC surfactants, tetraethyleneglycol mono-1,1-dihydrotridecafluoroheptyl ether (pFC7E4), and its ω-hydrogenated analogue, tetraethyleneglycol mono-1,1,7-trihydrododecafluoroheptyl ether (FC7E4), it was found that the existence of a terminal dipole lowers the surface density and increases the critical micelle concentration. Furthermore, the adsorption of 1*H*,1*H*-perfluorononanol (FDFC9OH) and its ω-hydrogenated analogue, 1*H*,1*H*,9*H*-perfluorononanol (HDFC9OH), at the hexane/water interface was investigated by evaluating the entropy, volume, and energy changes of adsorption to examine the effect of the ω-dipole on the state and molecular orientation in the adsorbed film.[4,5] It was suggested that FDFC9OH molecules orient almost normal to the interface, while HDFC9OH ones tilt around 15° from the interface normal

Received: September 27, 2012
Revised: October 22, 2012
Published: October 30, 2012

dx.doi.org/10.1021/jp309589f | J. Phys. Chem. B 2012, 116, 13739−13748

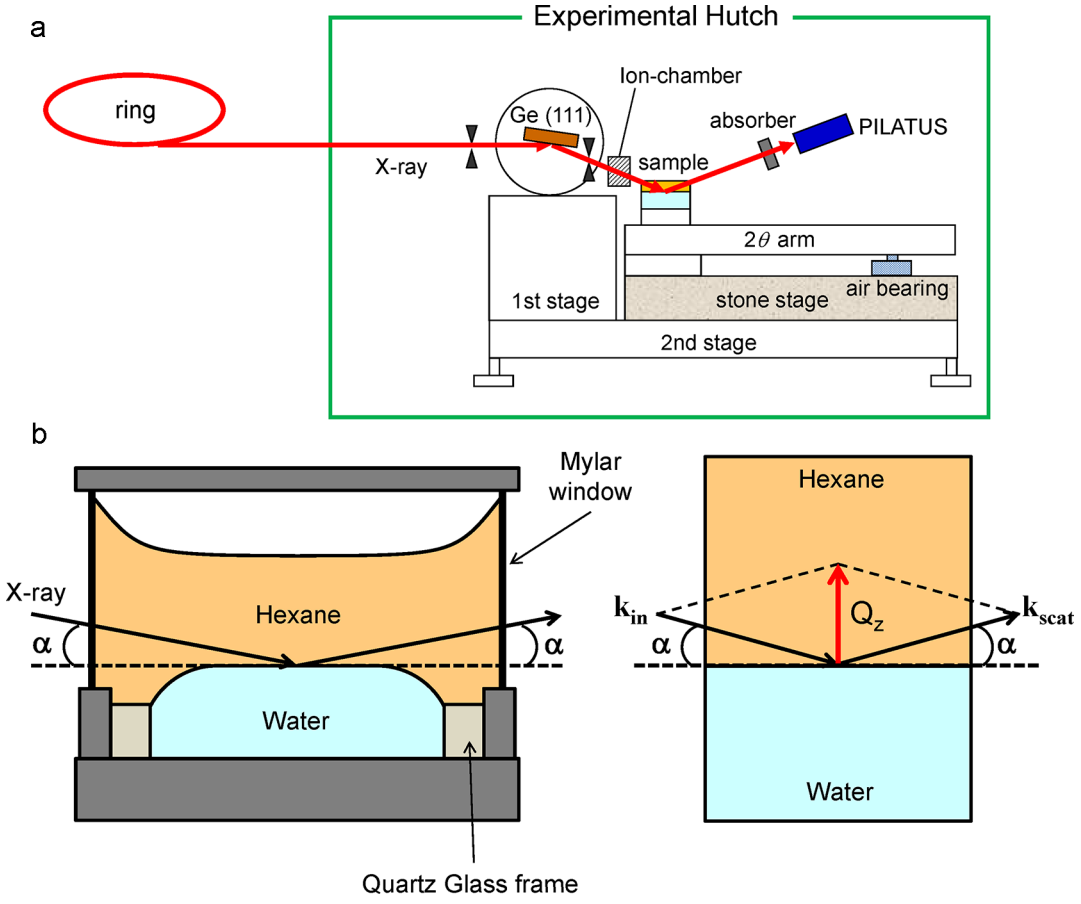

Figure 1. (a) Schematic illustration of the liquid surface spectrometer at BL37XU in SPring-8. (b) Schematic illustration of the XR cell (left) and the kinematics of reflectivity (right).

for ω-dipoles to interact effectively with water molecules and to reduce the electrostatic repulsion between neighbors in the interfacial region.

The mutual interaction between the adsorbed molecules affects appreciably the structure and the miscibility of molecules in the adsorbed film. Study on the adsorption of the 1*H*,1*H*-2*H*,2*H*-perfluorodecanol (FC10OH)−1-icosanol (C20OH) mixture at the hexane/water interface showed that both molecules are practically immiscible in the condensed film primarily due to weaker interaction between FC10OH and C20OH molecules than those between the same species.[8,9] XR measurement showed that FC10OH molecules are densely packed like a two-dimensional solid, and C20OH ones are in a liquid ordering just above the freezing point.[10−12] Furthermore, it was found that FC10OH forms a condensed-phase domain coexisting with very low density gaseous film in the expanded state.[11]

The effects of rigidity of the FC chain and two hydroxyl groups at both ends of the hydrophobic chain on the structure of adsorbed film were also studied in the adsorbed film of 1*H*,1*H*,10*H*,10*H*-perfluorodecane-1,10-diol (FC10diol) at the hexane/water interface.[13,14] One of the important findings was that FC10diol molecules form a condensed monolayer with molecular orientation parallel to the interface, which is in striking contrast to the wicket-like conformation of bola-type surfactants with a flexible HC chain at the air/water and oil/water interfaces.[15−17] Another noticeable point was that FC10diol molecules spontaneously pile on the condensed monolayer and form a multilayer. These film states are stabilized by hydrogen bonding between the hydroxyl group and water molecule and by that between hydroxyl groups facing each other.

Spontaneous multilayer formation at soft interfaces is a novel phenomenon, and some researchers have investigated the structure and property of the multilayer at the aqueous surfactant solution surface.[18−20] Kawai et al. studied the surface adsorbed film of the mixed sodium dodecyl sulfate (SDS) and cetylpyridinium chloride (CPC) system by infrared external reflection spectroscopy. It was claimed that the adsorbed film in a limited SDS composition range, $X_{SDS} \approx 0.6-0.7$, has multilayer structure, which is formed in a fast single layer formation followed by slow molecular piling.[19] Since the multilayer formation was not observed in the pure component systems, it would be related to the formation of an ion pair between anionic dodecyl sulfate and cationic cetylpyridinium ions. However, a mechanism of multilayer formation is still unknown.

In this study, we aim at discussing a novel multilayer formation induced in the mixed system of FC compounds, one of which exhibits negative adsorption at the hexane/water interface, from the viewpoint of molecular interaction and miscibility of molecules at the hexane/water interface by interfacial tensiometry and XR. We employed two kinds of mixed systems: 1*H*,1*H*,2*H*,2*H*-perfluorododecanol (FC12OH)−1*H*-perfluorodecane (HFC10) (System A) and 1-icosanol (C20OH)−HFC10 (System B). HFC10 has a terminal dipole by the substitution of a fluorine atom at the terminal position of the molecule into a hydrogen atom. The

dx.doi.org/10.1021/jp309589f | J. Phys. Chem. B 2012, 116, 13739−13748

interfacial tension between the hexane solution and water was measured as a function of the total molality and the composition of HFC10 in the mixture. The phase diagram of adsorption (PDA) was constructed and compared between the two systems. XR was applied to the adsorbed films of both systems, and the electron density profile along the interface normal was determined to know the film structure. The information from PDA and electron density profile is examined complementarily to elucidate the structure of the multilayer and to deduce the mechanism of the multilayer formation.

EXPERIMENTAL SECTION

Materials. 1*H*,1*H*,2*H*,2*H*-Perfluorododecanol (FC12OH; 98%, Azumax Co. Ltd.) was recrystallized twice from chloroform solution. 1-Icosanol (C20OH; 98%, Aldrich Chemical Co. Ltd.) was recrystallized twice from chloroform solution and then once from hexane solution. 1*H*-Perfluorodecane (HFC10; 98%, Azumax Co. Ltd.) was purified by distillation under reduced pressure and then by recrystallization once from chloroform solution. Their purities were checked by gas–liquid chromatography and also by observing no time dependence of interfacial tension between their hexane solution and water.

Hexane (99+% grade, Aldrich Chemical Co. Ltd.) distilled once and water produced by the Millipore Milli-Q system were used for measurement.

Interfacial Tensiometry. The interfacial tensions γ between hexane solution and water were measured as a function of the total molality m and the composition of HFC10 in the bulk solution X_2 at 298.15 K under atmospheric pressure by the pendant drop method based on the analysis of the drop shape.[21] Here, m and X_2 are defined, respectively, by

$$m = m_1 + m_2 \tag{1}$$

and

$$X_2 = m_2/m \tag{2}$$

where m_1 and m_2 are, respectively, the molalities of the first (FC12OH in system A, C20OH in system B) and the second component (HFC10) in the hexane solution. For the calculation of γ values, the densities of pure hexane and water were used instead of those of the hexane solution and water being in equilibrium with each other, because the concentration is sufficiently low and the mutual solubility between the two phases is negligibly small. The error in γ value was estimated to be within ± 0.05 mN m^{-1}.

X-ray Reflectometry. X-ray reflectivity of the hexane solution/water interface was measured at the beamline BL37XU in SPring-8 by using a liquid surface spectrometer described schematically in Figure 1(a).[22] The X-ray beam is monochromatized to 25 keV by a Si(111) double crystal monochromator. The incident angle of the X-ray beam to the sample interface is adjusted by a Ge(111) crystal. A slit placed upstream of the Ge crystal determines the incident beam size in the vertical direction to 15 μm. The beam is focused to about 200 μm in the horizontal direction at the sample position by an upstream mirror. The footprint on the sample interface is around 2 cm along the beam path at the incident angle of 0.05°. The incident beam flux is monitored by a N_2 gas ion chamber. The slit with a vertical gap of 2 mm was placed downstream of the cell to reduce the background scattering from bulk phases. The intensity of the reflected beam was detected by a two-dimensional pixel detector (PILATUS 100K; DECTRIS Ltd.) equipped with copper–aluminum absorbers to reduce the X-ray photons incident on the detector to optimum amounts.

Here, the kinematics of reflectivity is described in Figure 1(b) together with the schematic illustration of the sample cell. The cell is made of stainless steel and equipped with two Mylar windows. In specular reflection conditions, the scattering vector $\mathbf{Q} = k_{scat} - k_{in}$ is only in the normal to the interface (z-direction) and given by $\mathbf{Q}_z = (4\pi/\lambda)\sin\alpha$, where λ (= 0.496 Å) is the X-ray wavelength used in the present study and α is the incident angle. The measurement was carried out at given m and X_2 under atmospheric pressure. Temperature was controlled in 298.15 ± 0.05 K by circulating the thermostatted water around the sample cell.

X-ray reflectivity $R(\mathbf{Q}_z)$ was measured as a function of the scattering vector $\mathbf{Q}_z$ to yield an electron density profile normal to the interface. Under the first Born approximation, $R(\mathbf{Q}_z)$ is given by[23,24]

$$\frac{R(\mathbf{Q}_z)}{R_F(\mathbf{Q}_z)} \cong \left| \frac{1}{\rho_w - \rho_h} \int \frac{d\langle\rho(z)\rangle}{dz} \exp(-i\mathbf{Q}_z z) dz \right|^2 \tag{3}$$

where $\rho(z)$ is the electron density profile averaged over the interfacial plane along with z-direction which is normal to the interface; ρ_w and ρ_h are, respectively, the electron densities of bulk water and hexane phases, and $R_F(\mathbf{Q}_z)$ is Fresnel reflectivity for an ideally smooth interface calculated by[24,25]

$$R_F(\mathbf{Q}_z) \approx \left| \frac{\mathbf{Q}_z - \mathbf{Q}_z^T}{\mathbf{Q}_z + \mathbf{Q}_z^T} \right|^2 \tag{4}$$

where $\mathbf{Q}_z^T$ is the z-component of the scattering vector with respect to the lower phase given by

$$\mathbf{Q}_z^T \approx \sqrt{\mathbf{Q}_z^2 - \mathbf{Q}^2} \tag{5}$$

Here, the total reflection of X-ray from the lower phase occurs for $\mathbf{Q}_z < \mathbf{Q}_c$, where the scatter vector at critical angle $\mathbf{Q}_c$ is calculated by using the difference of bulk densities $\Delta\rho$ (= $\rho_w - \rho_h$) as $\mathbf{Q}_c \approx (\pi\Delta\rho r_e)^{1/2}$, where r_e is the classical electron radius r_e = 2.818 fm.

The adsorbed films at the hexane/water interface are modeled by n slabs. Interfaces at the top and bottom of each slab will fluctuate with thermally exited capillary waves,[26,27] which broadens the interface with an error function of interfacial roughness σ. Thus, the electron density for the n-slab model is given by

$$\langle\rho(z)\rangle = \frac{1}{2}(\rho_w + \rho_h) + \frac{1}{2}\sum_{i-0}^{n}(\rho_i - \rho_{i+1})\mathrm{erf}\left(\frac{z + \sum_{j=0}^{i} L_i}{\sqrt{2}\sigma}\right) \tag{6}$$

with

$$\mathrm{erf}(z) = \frac{2}{\sqrt{\pi}} \int_0^z e^{-t^2} dt \tag{7}$$

where ρ_i and L_i are the electron density and thickness of slab i, respectively.

The interfacial roughness σ is usually considered to be the combination of two different contributions: the intrinsic profile width σ_0 and the resolution-dependent capillary wave contribution σ_{cap}. In the hybrid model, the interfacial roughness

dx.doi.org/10.1021/jp309589f | J. Phys. Chem. B 2012, 116, 13739–13748

is described as $\sigma^2 = \sigma_0^2 + \sigma_{cap}^2$. The Buff, Lovett, and Stillinger capillary wave theory[26] predicts σ_{cap} as

$$\sigma_{cap}^2 = \frac{k_B T}{2\pi} \int_{q_{min}}^{q_{max}} \frac{q}{\gamma q^2 + \Delta d_m g} dq \approx \frac{k_B T}{2\pi\gamma} \ln\left(\frac{q_{max}}{q_{min}}\right) \quad (8)$$

where γ is the interfacial tension of the hexane/water interface, $k_B T$ is the Boltzman constant times the temperature, Δd_m (= $d_w - d_h$) is the difference of mass densities between two bulk phases, g is the gravitational acceleration, q_{min} (= $(2\pi/\lambda)\Delta\beta \sin\alpha$) with the angular acceptance of the detector $\Delta\beta = 6.37 \times 10^{-4}$, and $\Delta d_m g \ll q_{min}^2$. q is the in-plane wave vector of the capillary waves. The limit, q_{max}, is determined by the cutoff for the smallest wavelength of capillary waves that the interface can support. We have chosen $q_{max} = 2\pi/l$ Å^{-1} where l is an approximate size of hexane molecule.

RESULTS AND DISCUSSIONS

In Figure 2 are shown the equilibrium interfacial tension γ vs total molality m curves of the FC12OH−HFC10 system

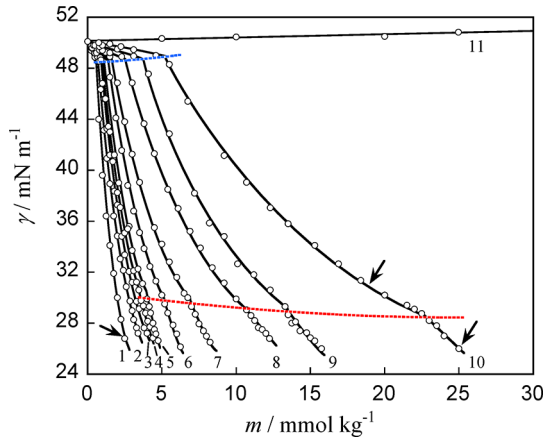

Figure 2. Interfacial tension vs total molality curves of System A at constant bulk composition: X_2 = (1) 0 (FC12OH), (2) 0.3, (3) 0.4, (4) 0.45, (5) 0.5, (6) 0.6, (7) 0.7, (8) 0.8, (9) 0.85, (10) 0.9, and (11) 1 (HFC10).

(System A) at constant bulk composition X_2. In the pure HFC10 system (X_2 = 1), the γ value increases slightly with increasing m, indicating the negative adsorption of HFC10 at the hexane/water interface. The γ values except at X_2 = 1, on the other hand, gradually decrease with increasing m, and the γ vs m curve has a distinct break point connected by a blue broken line at a low concentration (first transition) due to the phase transition in the adsorbed film. The break point of the pure FC12OH system (curve 1) was assigned as a phase transition between the gaseous and condensed monolayers in our previous studies.[28,29] In the mixed system, the shape of the curves at low X_2 (≤0.4) is very similar to that of pure FC12OH. One of the remarkable findings is that another break (second transition), which is traced by a red broken line, appeared on the curves at high concentrations in a limited X_2 range from 0.45 to 0.9.

The interfacial tension γ^{eq} and the total molality m^{eq} at the break points are plotted against X_2 in Figures 3(a) and 3(b), respectively. In Figure 3(b) are also shown the molality of FC12OH m_1^{eq} vs X_2 plots. The γ^{eq} value at the first transition is almost constant against X_2, and that at the second transition

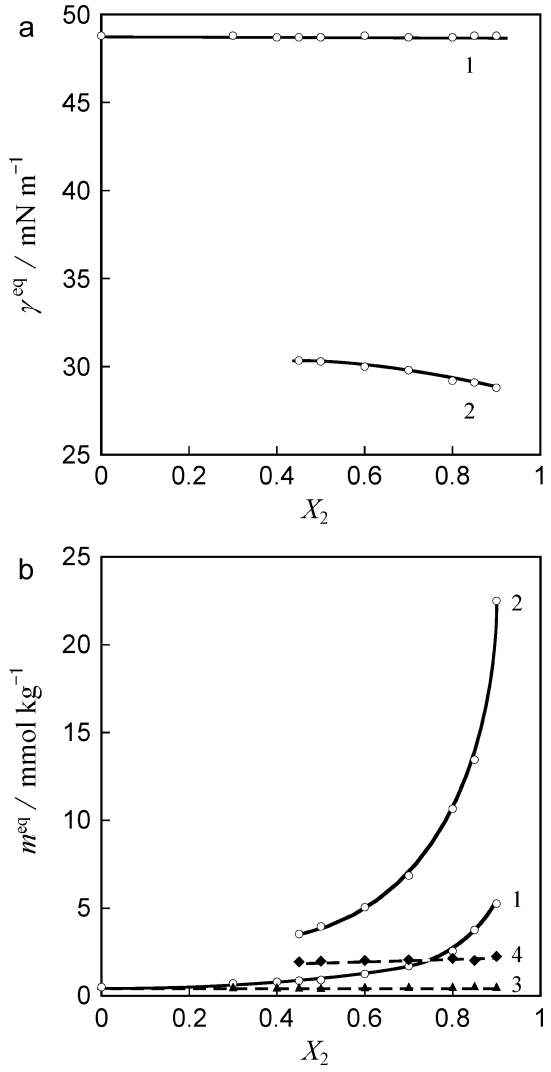

Figure 3. (a) Interfacial tension at the phase transition point vs bulk composition curves and (b) total molality at the phase transition point vs bulk composition curves: (1) gaseous−condensed monolayer transition, (2) condensed monolayer−multilayer transition, (3) m_1^{eq} vs X_2 at the gaseous−condensed monolayer transition, (4) m_1^{eq} vs X_2 at the condensed monolayer−multilayer transition.

decreases with increasing X_2. The m^{eq} values at both transitions increase with increasing X_2. On the other hand, the m_1^{eq} value at the first transition is almost constant against the variation of X_2, while that at the second transition increases slightly with increasing X_2; the mixing of HFC10 with FC12OH affects the second phase transition. We will refer to this in the latter part.

Here we briefly introduce the thermodynamic equations for analyzing the interfacial tension data. The total differential of γ for binary nonionic−nonionic mixtures is expressed as a function of temperature T, pressure p, and chemical potential of solute i, μ_i (i = 1, 2) by[30,31]

$$d\gamma = -s^H dT + v^H dp - \Gamma_1^H d\mu_1 - \Gamma_2^H d\mu_2 \quad (9)$$

where s^H, v^H, and Γ_i^H are the interfacial excess entropy, volume, and the number of moles of solute i per unit area defined with reference to the two dividing planes making the excess numbers of moles of water and hexane zero, concurrently. Assuming that the hexane solution is ideally dilute and substituting the total

dx.doi.org/10.1021/jp309589f | J. Phys. Chem. B 2012, 116, 13739−13748

differential of chemical potential of each component into eq 3, we have

$$d\gamma = -\Delta s dT + \Delta v dp - \Gamma^{H}(RT/m)dm - RT\Gamma^{H}[(X_2^{H} - X_2)/X_1X_2]dX_2 \quad (10)$$

where Δs and Δv are, respectively, the entropy and volume changes associated with adsorption, Γ^{H} the total interfacial density, and X_2^{H} the composition of HFC10 in the adsorbed film defined, respectively, by

$$\Delta y = y^{H} - \Gamma_1^{H} y_1^{O} - \Gamma_2^{H} y_2^{O}, \quad y = s, v \quad (11)$$

$$\Gamma^{H} = \Gamma_1^{H} + \Gamma_2^{H} \quad (12)$$

and

$$X_2^{H} = \Gamma_2^{H}/\Gamma^{H} \quad (13)$$

where s_i^{O} and v_i^{O} are the partial molar entropy and volume of solute i in the solution, respectively.

To characterize the state of the adsorbed film, first, the total interfacial density Γ^{H} was calculated by applying the equation

$$\Gamma^{H} = -(m/RT)(\partial\gamma/\partial m)_{T,p,X_2} \quad (14)$$

to the γ vs m curves in Figure 2. The results are shown as the Γ^{H} vs m curves in Figure 4. The Γ^{H} values except for the pure

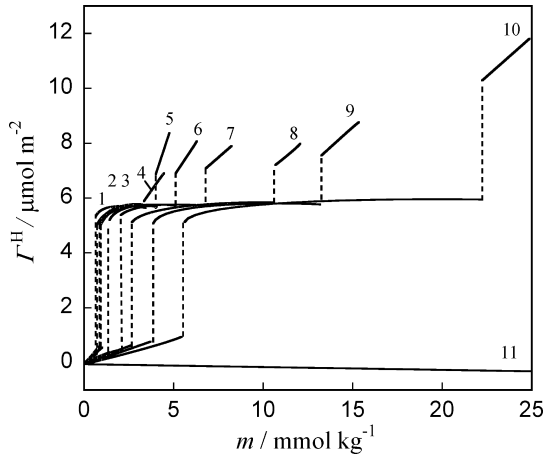

Figure 4. Total interfacial density vs total molality curves of System A at constant bulk composition: X_2 = (1) 0 (FC12OH), (2) 0.3, (3) 0.4, (4) 0.45, (5) 0.5, (6) 0.6, (7) 0.7, (8) 0.8, (9) 0.85, (10) 0.9, (11) 1 (HFC10).

HFC10 system increase with increasing m and change discontinuously from a relatively small value (at most 1 μmol m^{-2}) to a large one (ca. 5.5 μmol m^{-2}) at the first phase transition points. Above the transition point, the Γ^{H} values converge into around 5.7 μmol m^{-2} which is almost equal to the Γ^{H} value in the condensed FC12OH monolayer.[28,29] The noticeable point is that the values above the second phase transition are 7−11 μmol m^{-2}, which is much larger than the saturated value in the condensed FC12OH monolayer (ca. 5.8 μmol m^{-2}), and increase further with increasing m.

Then, it is advantageous to draw the interfacial pressure π vs the mean area per adsorbed molecule A curves to elucidate the film state more clearly. The π and A values are calculated, respectively, by the equations

$$\pi = \gamma^{0} - \gamma \quad (15)$$

and

$$A = 1/N_A\Gamma^{H} \quad (16)$$

where γ^{0} is the interfacial tension between pure hexane and water and N_A is Avogadro's number. The π vs A curves at constant X_2 except at X_2 = 1 are shown in Figure 5. A smaller A

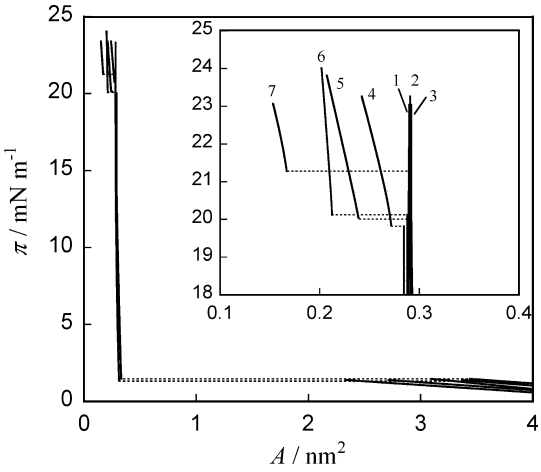

Figure 5. Interfacial pressure vs mean area per molecule curves of System A at constant bulk composition: X_2 = (1) 0 (FC12OH), (2) 0.3, (3) 0.4, (4) 0.45, (5) 0.6, (6) 0.85, (7) 0.9.

and a higher π region are magnified in the inset. The curves below X_2 = 0.4 consist of two parts and those above 0.45 three parts connected by discontinuous changes. In the intermediate state, the slope of the curve is almost vertical, and the A value is around 0.28−0.30 nm^2 which is very close to the cross-sectional area of the FC chain. Taking note of the previous result that the adsorbed FC12OH film shows a phase transition from the gaseous to the condensed monolayer, we conclude that the condensed monolayer is formed above the first phase transition point in the mixed system. Above the second transition, the A value is less than 0.28 nm^2 and decreases further with increasing π. Since the total interfacial density in this state is much larger than that of the condensed monolayer, it is likely that molecules pile spontaneously on the condensed monolayer and form the multilayer at the interface.

In the case of the C20OH−HFC10 system (System B), the γ vs m curves at given X_2 are shown in Figure 6. The γ values except at X_2 = 1 (pure HFC10) gradually decrease with increasing m, and the γ vs m curves have a distinct break point at low concentrations due to the phase transition in the adsorbed film. The break point on the curve of pure C20OH (curve 1) corresponds to the phase transition between the expanded and condensed monolayers.[8] Furthermore, it should be noted that no additional break was observed even at high concentration close to the solubility limit of C20OH in the hexane solution, which is very different from the finding that the additional break was observed on the γ vs m curve of System A.

The π vs A curves were drawn at given X_2 except at X_2 = 1 in Figure 7. The curves consist of two parts connected by a discontinuous change at the phase transition point. The curves above the transition are almost vertical, indicating that the compressibility of the film is extremely low. The A value in this region is around 0.18 nm^2, which is nearly equal to the cross-

dx.doi.org/10.1021/jp309589f | J. Phys. Chem. B 2012, 116, 13739−13748

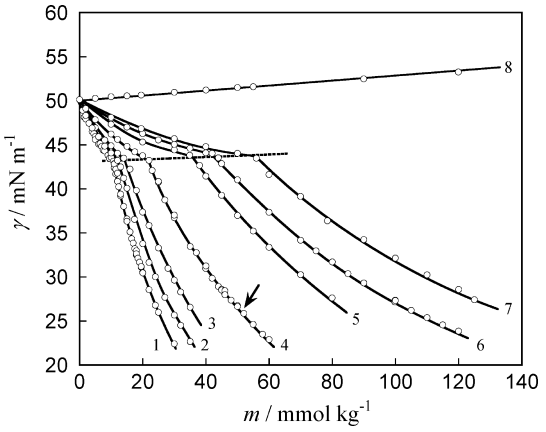

Figure 6. Interfacial tension vs total molality curves of System B at constant bulk composition: X_2 = (1) 0 (C20OH), (2) 0.15, (3) 0.3, (4) 0.5, (5) 0.7, (6) 0.75, (7) 0.8, (8) 1 (HFC10).

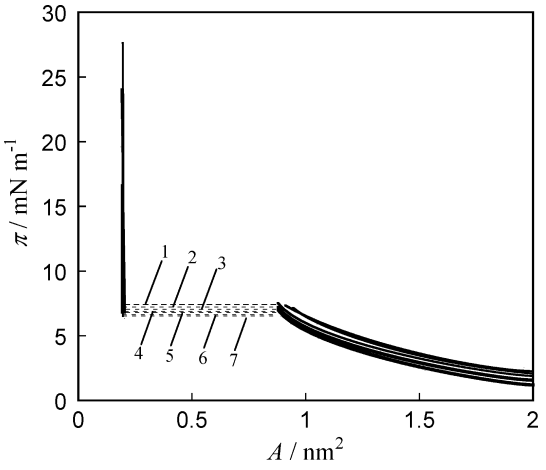

Figure 7. Interfacial pressure vs mean area per molecule curves of System B at constant bulk composition: X_2 = (1) 0 (C20OH), (2) 0.15, (3) 0.3, (4) 0.5, (5) 0.7, (6) 0.75, (7) 0.8.

sectional area of the HC chain, and thus it is expected that the molecules are densely packed with each other. Taking note of our previous conclusion that a phase transition from the expanded to the condensed monolayer takes place in the adsorbed C20OH film,[8] it is suggested that the adsorbed film of System B shows a phase transition between the expanded and the condensed monolayers.

Since the molecular piling on the condensed monolayer is induced only in a limited X_2 range of System A even though the condensed monolayer is formed in both Systems A and B, there should be a crucial difference in the miscibility of molecules in the adsorbed films between the two systems.

Phase Diagram of Condensed Monolayer. The miscibility of molecules in the adsorbed film was examined by constructing the phase diagram of adsorption (PDA), which provides a quantitative relation of the compositions between the bulk phase and the adsorbed film in equilibrium with each other. The composition of HFC10 in the adsorbed film X_2^H was calculated by applying the equation[31]

$$X_2^H = X_2 - (X_1X_1/m)(\partial m/\partial X_2)_{T,p,\gamma} \quad (17)$$

to the m vs X_2 curves at given γ. The results obtained in monolayer states are shown as the m vs X_2^H curves together with the corresponding m vs X_2 curves in Figure 8(a) for System A and in Figure 8(b) for System B. The chain-dotted line

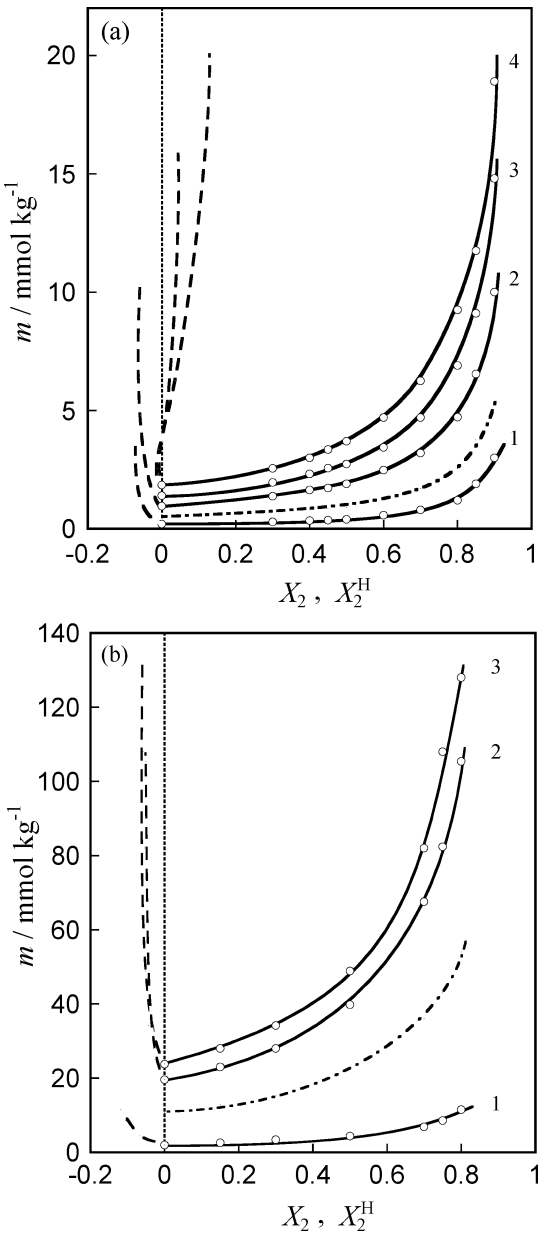

Figure 8. Phase diagram of adsorption: (—) m vs X_2 curve, (- - -) m vs X_2^H curve, (- · -) m^{eq} vs X_2 curve; (a) System A, γ = (1) 49.5, (2) 40, (3) 35, (4) 31 mN m^{-1}; (b) System B, γ = (1) 48, (2) 31, (3) 27 mN m^{-1}.

represents the m^{eq} vs X_2 curve for the gaseous–condensed monolayer transition of System A and that for the expanded–condensed monolayer transition of System B. In System B, it is clearly seen that the X_2^H values are negative in both expanded and condensed states. The negative X_2^H indicates that HFC10 molecules are expelled from the interfacial region and immiscible with C20OH in the adsorbed film. This is primarily due to the weak interaction between C20OH and HFC10 molecules compared to those between the same ones.

In System A, on the other hand, the X_2^H value in the condensed monolayer increases with decreasing γ and becomes positive below γ = 35 mN m^{-1} which is close to the γ value at the second phase transition point. This is in striking contrast to

dx.doi.org/10.1021/jp309589f | J. Phys. Chem. B 2012, 116, 13739–13748

Table 1. Samples Studied by X-ray Reflectivity Measurement at 298.15 K[a]

system	film state	X_2	m (mmol kg^{-1})	X_2^H	γ (mN m^{-1})	Γ^H (μmol m^{-2})
A-1 (FC12OH)	C	0	2.75	0	27.0	5.5
A-2 (FC12OH−HFC10)	C	0.9	19.0	0.15	31.0	5.5
A-3 (FC12OH−HFC10)	M	0.9	25.0	0.13	26.0	11
B (C20OH−HFC10)	C	0.5	50.0	∼ 0	26.5	8.4

[a]C: condensed monolayer, M: multilayer.

the negative X_2^H in the condensed monolayer of System B even at very low γ (PDA at 27 mN m^{-1} in Figure 8(b)). The positive X_2^H indicates the mixing of HFC10 with FC12OH in the condensed monolayer at which the molecules are densely packed with each other mainly due to favorable interaction between FC chains. Furthermore, it should be emphasized that the X_2^H value is positive in $0.45 \leq X_2 \leq 0.9$ in which the multilayer formation was found in System A; the multilayer formation seems to synchronize with the existence of HFC10 molecules in the condensed monolayer. Thus, it is necessary to examine the effect of the structure of the condensed monolayer on the multilayer formation.

For doing this, we employed four samples with different combinations of m and X_2 as indicated by arrows in Figures 2 and 6 for performing X-ray reflectivity (XR) measurement. The experimental conditions and the film states of these samples are summarized in Table 1.

Structure of the Condensed Monolayer. First of all, we refer to the XR results about the condensed monolayer of pure FC12OH (m = 2.75 mmol kg^{-1}, X_2 = 0) and that of System A with $X_2^H \approx 0.15$ (m = 19 mmol kg^{-1}, X_2 = 0.9). In Figures 9(a) and (b) are shown the reflectivity normalized by Fresnel reflectivity R/R_F vs scattering vector $\mathbf{Q}_z$ plots obtained at X_2 = 0 and X_2 = 0.9, respectively. It is realized that the shape of the plot is very similar to each other; both plots have a maximum around $\mathbf{Q}_z \sim 0.18$ Å. Taking account of the fact that the R/R_F values from the condensed monolayer of FC alcohols were well fitted by using a one-slab model since the electron density of the FC chain is much larger than that of the water phase and the contrasts of electron density of the hydrophilic group ($-CH_2CH_2OH$) against the FC chain and water phase are hidden by interfacial roughness σ.[10,11] Thus, we employed the one-slab model with uniform electron density and thickness for analyzing the X-ray reflectivity from the condensed monolayer of System A. In this model, the slab thicknesses L_1 and the electron density of the layer normalized by the electron density of water ρ_1/ρ_w were used as fitting parameters under the fixed σ as the capillary wave roughness. The fitting curves are shown by dotted lines, and the corresponding electron density profiles normal to the interface are drawn in the inset. The fitted parameter values are summarized in Table 2. The slab thicknesses of System A-1 and A-2 are almost the same and are very close to the molecular length of HFC10 and that of the FC part of the FC12OH molecule. Furthermore, the electron density profiles are also very similar to each other. Since the difference in electron densities between perfluorodecane (0.641 e$^-$ Å^{-3}) and HFC10 (0.637 e$^-$ Å^{-3}) is very small, it is hard to distinguish HFC10 from FC12OH in the adsorbed film by XR measurement. Instead of this, taking note of the thermodynamic information from the PDA that HFC10 molecules are miscible with FC12OH in the condensed monolayer, we can say that HFC10 molecules as well as FC12OH ones orient perpendicular to the interface and are densely packed with FC12OH in the condensed monolayer.

The R/R_F values obtained from the condensed monolayer at m = 50 mmol kg^{-1} and X_2 = 0.5 of System B are plotted against $\mathbf{Q}_z$ in Figure 9(c). The oscillation in R/R_F value clearly appeared on the plots, suggesting the presence of well-ordered interfacial structure such as a condensed monolayer at the interface. In our previous study on the adsorbed film of C20OH at the hexane/water interface by XR measutement,[11,12] the R/R_F vs $\mathbf{Q}_z$ plots for the condensed monolayer were fitted very well by using the two-slab model in which the adsorbed film is assumed to have a structure consisting of two slabs with different electron densities and thicknesses. The normalized electron density and thickness values obtained are listed in Table 2. The electron density of the upper slab (ρ_2/ρ_w = 0.8) agreed well with the density of 0.81 for the bulk liquid alkane just above the freezing point. This indicated a liquid ordering of the hydrophobic chains of C20OH molecules in the condensed monolayer at the hexane/water interface.

As we have already shown, the PDA in the condensed monolayer of System B (Figure 8(b)) suggested that the condensed monolayer consists of almost C20OH molecules. Thus, the primary choice for fitting the R/R_F vs $\mathbf{Q}_z$ plot is to employ the two-slab model. The fitted curve is shown by a dotted line in Figure 9(c), and the fitted parameters are listed in Table 2. The electron density profile normal to the interface is illustrated in the inset. The values of electron density and slab thickness are close to those of the pure C20OH condensed monolayer. This manifests that HFC10 molecules are practically immiscible with C20OH ones in the condensed monolayer, and the packing and orientation of C20OH molecules are almost the same as those in the pure C20OH condensed monolayer.

Phase Diagram of the Multilayer of System A. According to the γ vs m curves in Figure 2, the condensed monolayer (C)−multilayer (M) phase transition disappeared in $X_2 < 0.45$. The change in the interfacial density $\Delta\Gamma^H = \Gamma^{H,M} - \Gamma^{H,C}$ and that in the film composition $\Delta X_2^H = \Delta X_2^{H,M} - \Delta X_2^{H,C}$ at the transition point were estimated from the Γ^H vs m curves and the equation

$$\Delta X_2^H = -(X_1X_2/RT)(1/\Gamma^{H,M} - 1/\Gamma^{H,C})(\partial\gamma^{eq}/\partial X_2)_{T,p} \quad (18)$$

respectively, and plotted against X_2 in Figure 10. It is realized that the absolute values of $\Delta\Gamma^H$ and ΔX_2^H decrease with decreasing X_2 and are close to 0 but slightly positive at X_2 = 0.45, indicating that the states of the condensed monolayer and the multilayer become similar with each other with decreasing X_2, and eventually the condensed monolayer−multilayer transition disappears in between X_2 = 0.4 and 0.45.

Figure 11 shows the PDA at γ = 28 mN m^{-1} (diagram 1) at which the adsorbed film takes the multilayer above X_2 = 0.45 and the condensed monolayer below 0.4, although the transition between the two film states is not obvious. The X_2^H value in the multilayer is positive at high X_2, suggesting that HFC10 molecules as well as FC12OH ones pile to form the

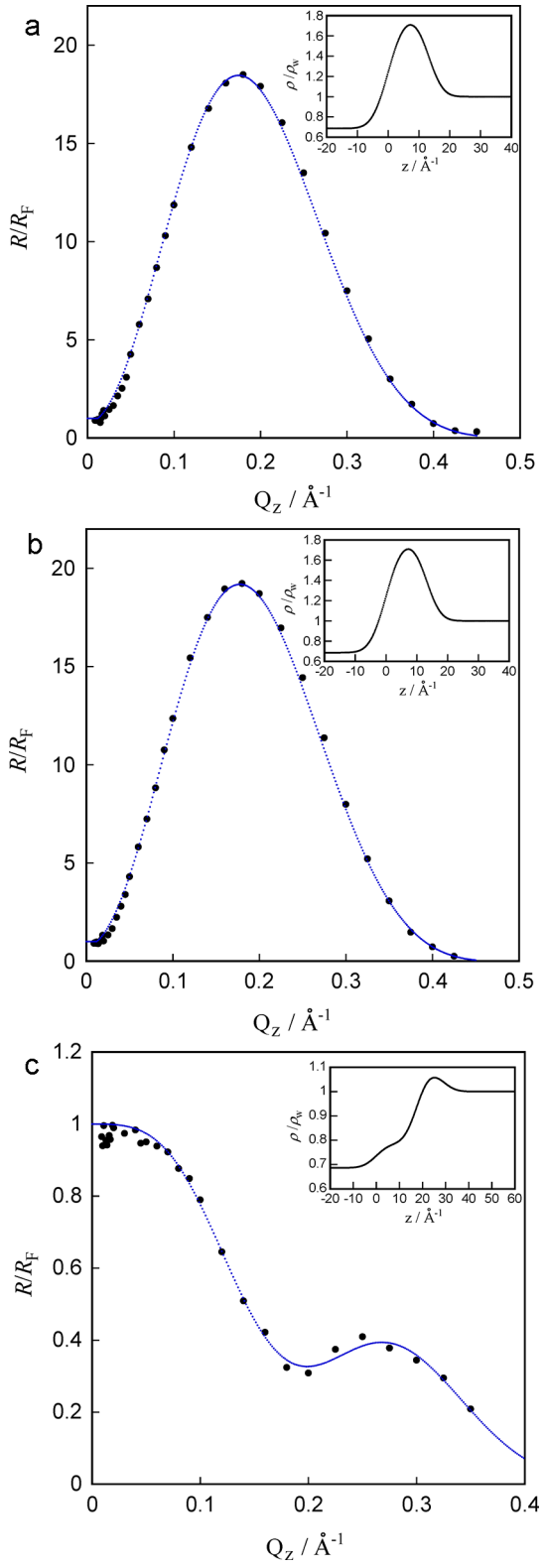

Figure 9. X-ray reflectivity normalized to Fresnel reflectivity vs scattering vector plot: (a) condensed monolayer of System A at m = 2.75 mmol kg^{-1} and X_2 = 0 (FC12OH), (b) condensed monolayer of System A at m = 19.0 mmol kg^{-1} and X_2 = 9, (c) condensed monolayer of System B at m = 50.0 mmol kg^{-1} and X_2 = 0.5. The dotted line is a fitted curve. The electron density profile along the interface normal is illustrated in the inset.

multilayer. Furthermore, the PDA of the condensed monolayer at γ = 31 mN m^{-1} is also shown for comparison. The X_2^H value is smaller in the multilayer than in the condensed monolayer, and thus FC12OH molecules preferentially pile to form a multilayer.

The piling of molecules is further examined by evaluating the ratio of the changes in the interfacial densities of individual components at the condensed monolayer−multilayer transition: $\Delta\Gamma_2^H/\Delta\Gamma_1^H = (\Gamma_2^{H,M} - \Gamma_2^{H,C})/(\Gamma_1^{H,M} - \Gamma_1^{H,C})$. Employing the expression for γ as a function of m_1 and X_2 at constant T and p given by

$$d\gamma^{eq} = -\Gamma^{H,C}(RT/m_1^{eq})dm_1^{eq} - \Gamma_2^{H,C}(RT/X_1X_2)dX_2 \quad (19)$$

and

$$d\gamma^{eq} = -\Gamma^{H,M}(RT/m_1^{eq})dm_1^{eq} - \Gamma_2^{H,M}(RT/X_1X_2)dX_2 \quad (20)$$

and eliminating $d\gamma^{eq}$ from the equations, we have

$$\Delta\Gamma_2^H/\Delta\Gamma_1^H = -(\partial m_1^{eq}/\partial X_2)_{T,p}/[(\partial m_1^{eq}/\partial X_2)_{T,p} + (m_1^{eq}/X_1X_2)] \quad (21)$$

The values were calculated by applying eq 21 to the m_1^{eq} vs X_2 curve shown in Figure 3 and plotted against X_2 in Figure 12. The ratio is negative, and the absolute value is much smaller than unity, indicating that Γ_1^H increases largely while Γ_2^H decreases slightly at the transition point. This demonstrates that FC12OH molecules pile preferentially to form the multilayer even though the multilayer formation is induced by the existence of HFC10 in the adsorbed film.

Structure of Multilayer of System A. The equilibrium R/R_F vs $\mathbf{Q}_z$ plot in the multilayer of System A-3 is shown in Figure 13. First, we tried to fit by the one-slab model in which the electron density ρ_1/ρ_w and thickness L_1 are employed as fitting parameters with fixed roughness σ. The fitting curve is drawn by the dotted black line, and the fitted parameters are listed in Table 2. Another option for fitting is the two-slab model in which the adsorbed film consists of two slabs with different electron densities and thicknesses. The result is shown by the dotted red line. The electron density and thickness values obtained are also summarized in Table 2, and the electron density profile normal to the interface is illustrated in the inset. It is clearly seen that the two-slab model gives better fitting than the one-slab model; the χ^2 value is smaller for the two-slab model than for the one-slab model. The thickness L_1 and the electron density ρ_1/ρ_w of the lower slab are close to those of the condensed monolayer, suggesting that the lower slab has a structure similar to the condensed monolayer. In the upper slab, on the other hand, the thickness L_2 is larger than the calculated molecular length of FC12OH and HFC10, and the electron density ρ_2/ρ_w is 0.75 which is much smaller than ρ_1/ρ_w but slightly larger than the electron density of bulk hexane, ρ_h/ρ_w = 0.68. These results indicate that a layer with relatively loose molecular packing is stacked on the condensed monolayer in which the molecules are densely packed with each other.

According to the above experimental findings obtained from the interfacial tension and XR measurements, let us expect the mechanism of the multilayer formation found in System A. The electron density profile of the condensed monolayer of System A indicated that the HFC10 as well as FC12OH molecules are densely packed with molecular orientation perpendicular to the

dx.doi.org/10.1021/jp309589f | J. Phys. Chem. B 2012, 116, 13739−13748

Table 2. Fitting Parameters Obtained by X-ray Reflectivity Measurement at 298.15 K[a]

					slab 1		slab 2	
system	film state	X_2	m (mmol kg^{-1})	σ (Å)	L_1 (Å)	ρ_1/ρ_w	L_2 (Å)	ρ_2/ρ_w
A-1	C	0	2.75	4.2	12.7	1.82		
A-2	C	0.9	19.0	4.0	13.2	1.79		
A-3	M	0.9	25.0	4.5	12.9	1.78	22.0	0.75
A-3	M	0.9	25.0	4.5	13.3	1.71		
B	C	0.5	50.0	4.5	10.7	1.09	17.6	0.78
[b]C20OH	C	0	15.0	4.7	8.0	1.15	17.0	0.80

[a]C: condensed monolayer, M: multilayer. [b]Measurement at 292.55 K.

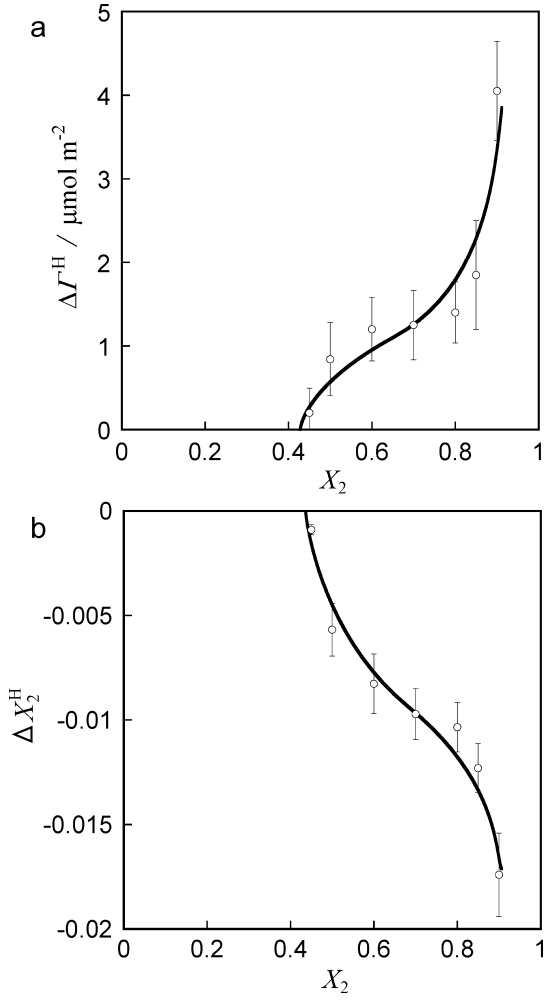

Figure 10. (a) Change in total interfacial density vs bulk composition curve at the condensed monolayer−multilayer transition. (b) Change in film composition vs bulk composition curve at the condensed monolayer−multilayer transition.

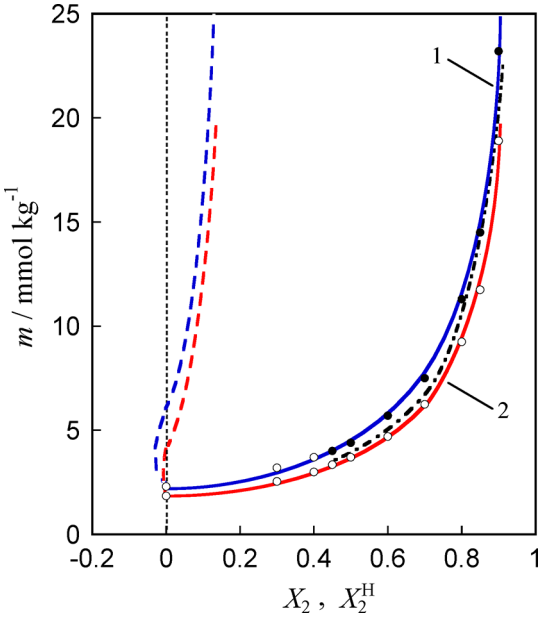

Figure 11. Phase diagram of adsorption of System A: (−) m vs X_2 curve, (- - -) m vs X_2^H curve; (○) condensed monolayer, (●) multilayer; γ = (1) 28, (2) 31 mN m^{-1}.

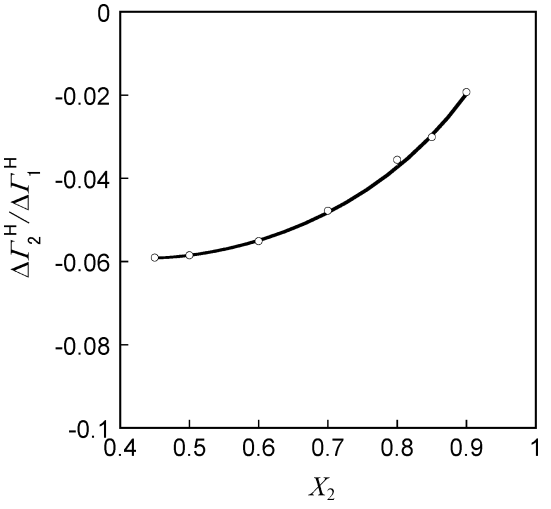

Figure 12. Ratio of the change in interfacial density of each component vs bulk composition curve at the condensed monolayer−multilayer transition point.

interface. Furthermore, it is expected that the ω-dipoles of HFC10 in the condensed monolayer are anchored at the interface to interact effectively with water molecules. Thus, one of the expected scenarios of molecular piling is as follows. HFC10 molecules in the condensed monolayer induce the piling of other HFC10 molecules by the interaction between ω-dipoles of HFC10 aligning the same direction.[32] Then, the other FC12OH laterally interacts with HFC10 and FC12OH by the dispersion interaction and hydrogen bonding to further induce molecular piling. Furthermore, the electron density profile in the multilayer of System A suggested that the molecular packing is much looser in the upper layer of the multilayer than in the condensed monolayer. Taking note of the facts that FC12OH preferentially piles on the condensed monolayer in which the composition of HFC10 is 0.15 at most,

dx.doi.org/10.1021/jp309589f | J. Phys. Chem. B 2012, 116, 13739−13748

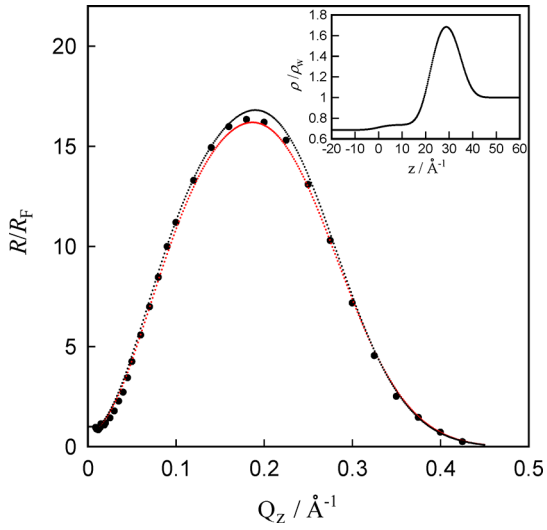

Figure 13. X-ray reflectivity normalized to Fresnel reflectivity vs scattering vector plot in multilayer: red dotted line is the fitted curve by the two-slab model and the black one by the one-slab model. The electron density profile along the interface normal is illustrated in the inset.

the molecular piling is expected to be induced in a limited region in the condensed monolayer. Thus, it is reasonable that the multilayer is heterogeneous in horizontal as well as in normal to the interface.

AUTHOR INFORMATION

Corresponding Author

*Prof. Dr. Takanori Takiue, Department of Chemistry, Faculty of Sciences, Kyushu University, Hakozaki 6-10-1, Higashi-ku, Fukuoka 812-8581, Japan. Phone: +81 92 642 2578. Fax: +81 92 642 2607. E-mail: t.takiue@chem.kyushu-univ.jp.

Notes

The authors declare no competing financial interest.

ACKNOWLEDGMENTS

This work was supported in part by the Grant-in-Aid for Scientific Research on Innovative Areas (Soft Interface Science) of the Ministry of Education, Culture, Sports, Science and Technology of Japan (No. 23106715). The X-ray reflectivity measurements were performed at BL37XU in SPring-8 under the approval of Japan Synchrotron Research Institute (Nos. 2010A1190, 2011A1202, and 2012A1203).

REFERENCES

(1) Kissa, E. *Fluorinated Surfactants and Repellents*; Surfactant Science Series, 2nd ed.; Marcel Dekker: New York, 2001; Vol 97.
(2) Krafft, M. P.; Goldmann, M. *Curr. Opin. Colloid Interface Sci.* **2003**, *8*, 243−250.
(3) Krafft, M. P.; Reiss, J. G. *Chem. Rev.* **2009**, *109*, 1714−1792.
(4) Takiue, T.; Hirose, D.; Murakami, D.; Sakamoto, H.; Matsubara, H.; Aratono, M. *J. Phys. Chem. B* **2005**, *109*, 16429−16434.
(5) Takiue, T.; Murakami, D.; Tamura, T.; Sakamoto, H.; Matsubara, H.; Aratono, M. *J. Phys. Chem. B* **2005**, *109*, 14154−14159.
(6) Downer, A.; Eastoe, J.; Pitt, A. R.; Simister, E. A.; Penfold, J. *Langmuir* **1999**, *15*, 7591−7599.
(7) Eastoe, J.; Paul, A.; Rankin, A.; Wat, R.; Penfold, J.; Webster, J. R. P. *Langmuir* **2001**, *17*, 7873−7878.
(8) Takiue, T.; Matsuo, T.; Ikeda, N.; Motomura, K.; Aratono, M. *J. Phys. Chem. B* **1998**, *102*, 4906−4911.
(9) Takiue, T.; Matsuo, T.; Ikeda, N.; Motomura, K.; Aratono, M. *J. Phys. Chem. B* **1998**, *102*, 5840−5844.
(10) Tikhonov, A. M.; Li, M.; Schlossman, M. L. *J. Phys. Chem. B* **2001**, *105*, 8065−8068.
(11) Pingali, S. V.; Takiue, T.; Luo, G.; Tikhonov, A. M.; Ikeda, N.; Aratono, M.; Schlossman, M. L. *J. Phys. Chem. B* **2005**, *109*, 1210−1225.
(12) Pingali, S. V.; Takiue, T.; Luo, G.; Tikhonov, A. M.; Ikeda, N.; Aratono, M.; Schlossman, M. L. *J. Dispersion Sci. Technol.* **2006**, *27*, 715−722.
(13) Takiue, T.; Fukuda, T.; Murakami, D.; Inomata, H.; Sakamoto, H; Matsubara, H.; Aratono, M. *J. Phys. Chem. C* **2008**, *112*, 5078−5084.
(14) Takiue, T.; Fukuda, T.; Murakami, D.; Sakamoto, H; Matsubara, H.; Aratono, M. *J. Phys. Chem. B* **2009**, *113*, 14667−14673.
(15) Merger, F. M.; Wrenn, S. *J. Phys. Chem.* **1974**, *78*, 1387−1390.
(16) Abid, S. K.; Hamid, S. M.; Sherrington, D. C. *J. Colloid Interface Sci.* **1987**, *120*, 245−255.
(17) Pal, R. P.; Chatterjee, A. K.; Chattoraj, D. K. *J. Colloid Interface Sci.* **1975**, *52*, 46−55.
(18) Penfold, J.; Sivia, D. S.; Staples, E.; Tucker, I.; Thomas, R. K. *Langmuir* **2004**, *20*, 2265−2269.
(19) Kawai, T.; Yamada, Y.; Kondo, T. *J. Phys. Chem. C* **2008**, *112*, 2040−2044.
(20) Takumi, H.; Noda, M.; Matsubara, H.; Takiue, T.; Aratono, M. *Chem. Lett.*, in press.
(21) Sakamoto, H.; Murao, A.; Hayami, Y. *J. Inst. Image Inf. Telev. Eng.* **2002**, *56*, 1643−1650.
(22) Yano, Y.; Uruga, T.; Tanida, H.; Toyokawa, H.; Terada, Y.; Yamada, H. *J. Synchrotron Radiat.* **2010**, *17*, 511−516.
(23) Pershan, P. S. *Faraday Discuss. Chem. Soc.* **1990**, *89*, 231−245.
(24) Zhang, Z.; Mitrinovic, D. M.; Williams, S. M.; Huang, Z.; Schlossman, M. L. *J. Chem. Phys.* **1999**, *110*, 7421−7432.
(25) Als-Nielsen, J.; Jacquemain, D.; Kjaer, K.; Leveiller, F.; Lahav, M.; Leiserowitz, L. *Phys. Rep.* **1994**, *246*, 251−313.
(26) Buff, F. P.; Lovett, R. A.; Stillinger, F. H. *Phys. Rev. Lett.* **1965**, *15*, 621−623.
(27) Wu, E. S.; Webb, W. W. *Phys. Rev. A* **1973**, *8*, 2065−2076.
(28) Hayami, Y.; Uemura, A.; Ikeda, N.; Aratono, M.; Motomura, K. *J. Colloid Interface Sci.* **1995**, *172*, 142−146.
(29) Takiue, T.; Yanata, A.; Ikeda, N.; Motomura, K.; Aratono, M. *J. Phys. Chem.* **1996**, *100*, 13743−13746.
(30) Motomura, K. *J. Colloid Interface Sci.* **1978**, *64*, 348−355.
(31) Aratono, M.; Villeneuve, M.; Takiue, T.; Ikeda, N.; Iyota, H. *J. Colloid Interface Sci.* **1998**, *200*, 161−171.
(32) *Intermolecular and Surface Forces*, 2nd ed.; Israelachivili, J. N., Ed.; Academic Press: London, 1992; Chapter 4.